Original Research Paper

Hybrid Multi-Layer Perceptron and Enhanced Edge-Free Active Contour Model Lung Nodule Detection Algorithm

Shengguang Peng

Department of Basic Teaching, Gandong University, Fuzhou Jiangxi, China

Abstract: A computer-assisted method is usually used to identify pneumoconiosis by segmenting and classifying the initial area of interest. The accuracy of current techniques for segmenting and classifying lung nodules is often suboptimal. Therefore, a hybrid Multi-Layer Perceptron (MLP) and enhanced edge-free active contour model (CV) algorithm are proposed to solve this problem. First, lung nodules are identified by the MLP to determine their locations and delineate their initial boundaries. CV is then used to automate segmentation and detect lung nodules quickly and accurately. Based on the LUNA16 dataset, the algorithm is trained and evaluated for more than 100 epochs, with 17 epochs achieving perfect accuracy. It is worth noting that only running the third epoch achieves 100% accuracy, proving its efficiency and effectiveness. The proposed method has greater accuracy than the comparing me.

Keywords: Pneumoconiosis, MLP, CV, Lung Nodule Detection

Introduction

Pneumoconiosis is a globally prevalent occupational disease (Lyu *et al.*, 2022), severe fibrosis of lung tissue caused by long-term inhalation of industrial dust. It accounts for a staggering 11,809 of the 15,407 new cases of occupational diseases in the China Health Report 2021 (National Health Commission of the People's Republic of China, 2022). Artificial Intelligence (AI) can assist in the diagnosis of pneumoconiosis to obtain rapid and accurate results. Xiang *et al.* (2019) made significant progress in clinical diagnosis by using various artificial intelligence technologies to conduct predictive models for lung nodules. Annarumma *et al.* (2019) validated Convolutional Neural Networks (CNN) systems for real-time classification of chest X-rays. None of these diagnoses can be made without image segmentation. The core of image segmentation is the technique and process of extracting the Region Of Interest (ROI) for unique parts (Li, 2022).

In medical image analysis, accurate segmentation is crucial for diagnosing diseases such as pneumoconiosis. Combined MLP (Manaswi, 2018) with the CV model (Chan and Vese, 2001), an advanced detection algorithm was developed. The algorithm was tested on the LUNA16 dataset (https://luna16.grand-challenge.org/) and showed good performance in recognizing lung nodules. The innovation of this algorithm lies in its ability to utilize the advantages of MLP and CV models to achieve high accuracy and efficiency. This study introduces auxiliary learning to enhance the MLP and employs the Additively Operable Splitting Operator (AOS) to improve the numerical computation. The operator can achieve 100% accuracy only in 3 iterations and maintains consistently high accuracy throughout the entire experiment process. This study not only breaks new ground in detection methods but also sets a new standard for speed and accuracy in medical image analysis.

Related Work

This section summarizes the existing research work in the MLP, ACM, and CV models for motivation.

MLP

Perceptron (Rosenblatt, 1958) is an algorithm to modify free parameters in neural networks. MLP is an artificial neural network characterized by a feedforward structure, which performs well in nonlinearly separable problems. It contains input, hidden, and output layers. As a generalized function approximator, MLP has similar structures with convolutional neural networks, both relying on backpropagation methods for training. In addition, MLP embodies a deep learning model that follows the principle of feature reuse (Bengio *et al.*, 2013), expanding the diversity of network output concepts and improving the efficiency of parameter usage. Let *f* be an s-shaped transfer function running inside a neuron and the input x_k, output y_i, $w_{kj}^{(2)}$ and $w_{ji}^{(1)}$ denote the weights corresponding to the connections from the input to hidden layers and the hidden to output layers, respectively. The output value is calculated as follows:

$$y_i = f(\sum_j w_{ji}^{(1)} f(\sum_k w_{kj}^{(2)} x_k)) \qquad (1)$$

MLP is an efficient classification algorithm that has been widely and successfully applied to a variety of medical challenges (Desai and Shah, 2021). Yan *et al.* (2022) introduced the TGMLP UNet model, a three-gate multilayer perceptron-based approach for medical image segmentation. The experimental results have shown that this model is better than other models in most evaluation metrics, highlighting its outstanding performance in the field.

Active Contour Model

The active Contour Model (ACM) proposed by Kass *et al.* (1988) has become a fundamental technique for image segmentation and remains an active area in computer vision research (Cootes *et al.*, 1995). Over the years, various adaptations have been proposed to enhance the capabilities of ACM. Ma *et al.* (2019) introduced an adaptive ACM based on local fitting, specifically for medical image segmentation. Dong *et al.* (2021) proposed an ACM driven by Self-Organizing Maps (SOM) and Akbari *et al.* (2021) first applied it to segment ORACM in COVID-19 CT images, achieving good results.

CV Model

The ACM algorithm has been improved from different perspectives. Mumford and Shah (1989) proposed a region-based level set method, i.e., the MS model. Chen and Vese proposed a simplified CV model, which belongs to the two-stage segmentation algorithm with a single-level set. Let Ω be a bounded open subset of R^2, $\varphi : \Omega \to R$ is the Lipschitz continuous level set function, contour curve, $\Gamma \subset \Omega, u : \Omega \to R, \Omega \subset R^2$ represents a grayscale image. The energy function of the CV model can be expressed as follows:

$$F(c_1, c_2, \varphi) = \mu \int_\Omega |\nabla H(\varphi(x,y))| dxdy + v \int_\Omega |H(\varphi(x,y))| dxdy$$
$$+ \lambda_1 \int_\Omega |u_0(x,y) - c_1|^2 H(\varphi(x,y)) dxdy + \lambda_2 \int_\Omega |u_0(x,y) - c_2|^2 \left(1 - H(\varphi(x,y))\right) dxdy \qquad (2)$$

H represents the unit step function; $\mu \geq 0, v \geq 0, \lambda_1 > 0, \lambda_2 > 0$ is a fixed coefficient; the average gray level Γ inside and outside of the curve is c_1 and c_2, respectively, and expressed as follows:

$$\begin{cases} c_1(\phi) = \dfrac{\int_\Omega u_0(x,y) H(\phi(t,x,y)) dxdy}{\int_\Omega H(\phi(t,x,y)) dxdy} \\ c_2(\phi) = \dfrac{\int_\Omega u_0(x,y) \left(1 - H(\phi(t,x,y))\right) dxdy}{\int_\Omega 1 - H(\phi(t,x,y)) dxdy} \end{cases} \qquad (3)$$

When the energy function reaches its minimum value, the segmentation contour converges to the true boundary of the image. Minimizing the energy function is usually achieved through the first-order variational splitting, from which the Euler-Lagrange equation can be obtained as follows:

$$\frac{\partial \varphi}{\partial t} = \delta(\varphi) \left[\mu \mathrm{div}\left(\frac{\nabla\varphi}{|\nabla\varphi|}\right) - v - \lambda_1 (u - c_1)^2 + \lambda_2 (u - c_2)^2 \right] \quad (4)$$

Research Motivation

Neural networks are categorized into shallow neural networks represented by MLP and deep neural networks represented by CNN. Although CNN has made significant progress in medical image segmentation, it still faces challenges in making further breakthroughs (Yan *et al.*, 2022). MLP, as a compact deep neural network with fast computation, powerful parallel processing, and superior all-connectivity unmatched by CNN, has become an important hotspot. Shi *et al.* (2022) introduced a fuzzy ACM by using multi-channel CNN for medical image segmentation. Ma *et al.* (2024) proposed an edge detection algorithm based on the Laplace operator (LOACM). Gao *et al.* (2024) proposed an enhanced segmentation method for pancreatic CT using the Superpixel Active Contour Model (SbACM) to improve the efficiency of conventional methods by addressing boundary leakage and slow contour evolution.

Drawing on these advances, MLP (which specializes in recognition and classification) is integrated with CV models (which are primarily used for segmentation) to present a synergistic approach, maximizing the advantages of both. This improved integration aims to leverage the complementary capabilities of MLP and CV models and surpass the inherent limitations of CNN, thereby making medical image analysis more efficient and accurate.

Materials and Methods

Feature Extraction

A vector transformation is performed based on the initial image to extract the feature vectors and then the problem is transformed into a boundary definition problem for feature space.

Basic Working Principle

As shown in Fig. (1), feature extraction is first performed on the positive case data to transform the initial dataset into a one-dimensional feature vector and ensure the full utilization of features. Subsequently, considering the generalization ability of the model integrated with the auxiliary learning task compared to the model without the auxiliary learning task (Lyu *et al.*, 2022), the obtained one-dimensional feature vectors are input into an MLP network with an auxiliary function header. The output in the middle layer of this MLP network is then utilized to augment the CV algorithm to build a preliminary target profile. Meanwhile, the final output of the MLP network pinpoints the region of suspected lung nodules. Finally, by reducing the internal energy, the initial contour facilitates a smooth inward contraction of the curve, achieving fast and accurate target contour segmentation as well as efficient and accurate positive case identification.
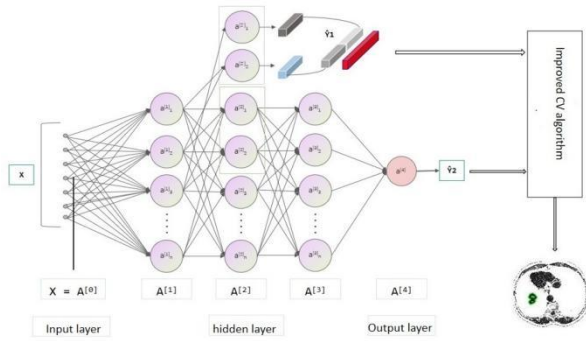
Fig. 1: Overall architecture diagram of the improved fusion MLP-CV

The proposed method simplifies the detection of lung nodules by integrating feature extraction, transformation, and neural network analysis. The combined module diagram of the MLP and CV models is shown in Fig. (2). The detailed steps are as follows: First, texture, shape, and pixel intensity features are extracted from ortho mosaic CT scanned images and then normalized to reduce the inter-image variance. PCA is used to reduce dimensionality and generate a one-dimensional feature vector, so as to improve the computational tractability and generality of the model. These vectors are processed by a Multilayer Perceptron (MLP) network equipped with a ReLU activation hidden layer and a Sigmoid output layer. An auxiliary learning task helps initialize the Chan-Vese (CV) model contours based on the intermediate output of the MLP. The final output of the MLP delineates the nodal regions through binary classification. The CV model is modified to improve its robustness to initial contour localization and handle images with noise and discontinuous edges. An Additive Operator Segmentation (AOS) operator is used to accelerate the evolution and an energy term is used to approximate the symbolic distance function, thereby improving the accuracy of segmentation. The algorithm first performs feature extraction, contour initialization, and nodal region identification through MLP analysis and then refines through iterative CV models until segmentation convergence is achieved.

Model Setup

Based on Kolmogorov's theorem, a three-layer neural network only containing input, hidden and output layers can map any data. If there are too many $many X \in R^l to Y \in R^m$ hidden layers (Zhang, 2002), it will increase the computational effort and increase the difficulty of parameter optimization, making the model difficult for training. Therefore, the number of hidden layers in the neural network is set to one (Peng, 2019). The activation function is selected as the Sigmoid function and the formula is as follows:

$$y = \frac{1}{1+e^{-x}} \qquad (5)$$
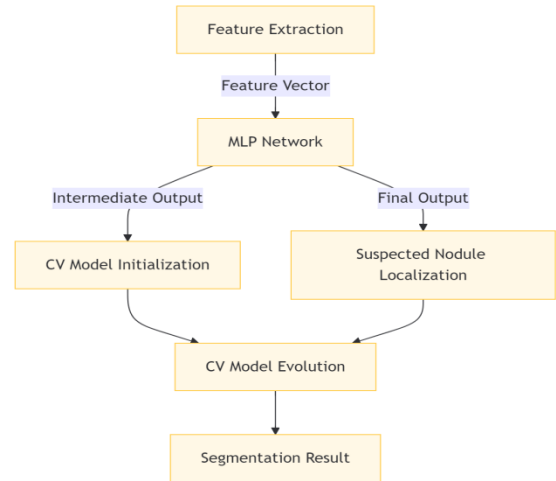
Fig. 2: Module combination diagram of MLP-CV

Improvement of the MLP Model

For example, the setting of MLP parameters requires many experiments to find relatively optimal results and lacks a reliable theoretical basis. It is highly dependent on the initial solution and is easy to falls into local optimization. Therefore, we made the following improvements. MLP is used to divide the feature space, introduce an auxiliary learning head (Fig. 3), and set classification loss and auxiliary learning regression loss, which are used for case identification and target detection region initialization, respectively. The classification formula of Loss is as follows:

$$H(y,p) = \sum_{k=1}^{K} -y_k \log(p_k)$$
$$= -(1 - \alpha + \frac{\alpha}{K})\log p_t - \frac{\alpha}{K} \sum_{i \neq t} \log p_i$$
$$(6)$$

That is, if the loss reaches the extremum point, smoothing cross-entropy loss can overcome cross-entropy loss selection by keeping the logit of correct and incorrect classes at a constant distance.

For the initialization of the target detection region, the following Huber Loss function is used:

$$L_\delta(y, f(x)) = \begin{cases} \frac{1}{2}(y - f(x))^2 & \text{for } |y - f(x)| \leq \delta \\ \delta|y - f(x)| - \frac{1}{2}\delta^2 & \text{otherwise} \end{cases} \qquad (7)$$

In terms of sensitivity to outliers in the data, the Huber loss is slightly worse than the squared error loss. However, when the value is 0, it is microscopic and essentially an absolute value; when the error is small, it becomes squared. This setting of the loss function is more favorable for the network to identify the target detection region.

The auxiliary network header is as follows:
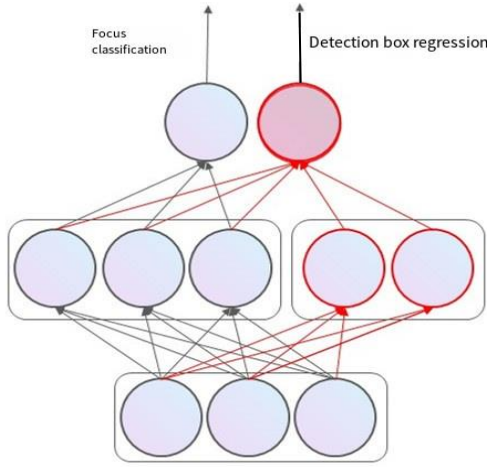
Fig. 3: Diagram of the secondary network header

Improved CV Model

This model is robust to initial contour locations and noisy, blurred, and discontinuous edge images. Abbas and Li (2023) proposed a locally enhanced Chan-Vese model (LECV) in 2024, which successfully segmented images with inhomogeneous intensity. However, the above methods have problems such as low accuracy of segmentation and blurred edges. Therefore, the following improvements are made.

Considering the actual planning and solving requirements, a simplified method and an iterative method are used to solve the specific CV model, and a numerical solving method is established. First, the Heaviside and Dirac functions are simplified:

$$H_\varepsilon(z) = \begin{cases} 1, \text{ if } z > \varepsilon \\ 0, \text{ if } z < -\varepsilon \\ \frac{1}{2}\left[1 + \frac{z}{\varepsilon} + \frac{1}{\pi}sin\left(\frac{\pi z}{\varepsilon}\right)\right], \text{ if } |z| \leq \varepsilon \end{cases} \quad (8)$$

$$\delta_\varepsilon(x) = H_\varepsilon^{'(x)} = \begin{cases} 1 \\ \frac{1}{2\varepsilon}\left[1 + \cos\left(\frac{\pi z}{\varepsilon}\right)\right], \text{ if } |z| < \varepsilon \end{cases}$$

Let $\varepsilon = 1e-5$, then the numerical method for calculating image curvature be established as follows:

$$Curvature\ K = div\left(\frac{\nabla\phi}{|\nabla\phi|}\right) = \frac{\phi_{xx}\phi_y^2 - 2\phi_{xy}\phi_x\phi_y + \phi_{yy}\phi_x^2}{(\phi_x + \phi_y)^{3/2}} \quad (9)$$

Let ϕ_x, ϕ_y and ϕ_{xy} is the difference calculation formula of ϕ, here the forward finite difference is used to obtain:

$$\begin{cases} \phi_x = \frac{\phi_{x+\Delta x,y} - \phi_{x,y}}{\Delta x} \\ \phi_y = \frac{\phi_{x,y+\Delta y} - \phi_{x,y}}{\Delta y} \\ \phi_{xy} = \frac{(\phi_{x+\Delta x,y+\Delta y} - \phi_{x,y+\Delta y}) - (\phi_{x+\Delta x,y} - \phi_{x,y})}{\Delta x\Delta y} \end{cases} \quad (10)$$

The number of spatial steps is ordered, then: $h = \Delta x = \Delta y = 1$:

$$\begin{cases} \phi_x = \phi_{x+1,y} - \phi_{x,y} \\ \phi_y = \phi_{x,y+1} - \phi_{x,y} \\ \phi_{xy} = \phi_{x+1,y+1} - \phi_{x,y+1} - (\phi_{x+1,y} - \phi_{x,y}) \end{cases} \quad (11)$$

The pair is discretized to facilitate subsequent iterative calculation ϕ:

$$\frac{\phi_{i,j}^{n+1} - \phi_{i,j}^n}{\Delta t} = \delta_h(\phi_{i,j}^n)\left[\frac{\mu}{h^2}(p \cdot L(\phi^n)^{p-1})\Delta_+^x\left(\frac{\Delta_+^x\phi_{i,j}^{n+1}}{\sqrt{(\Delta_+^x\phi_{i,j}^n)^2/(h^2) + (\phi_{i,j+1}^n - \phi_{i,j-1}^n)^2/(2h)^2}}\right)\right.$$

$$+ \frac{\mu}{h^2}(p \cdot L(\phi^n)^{p-1})\Delta_+^y\left(\frac{\Delta_+^y\phi_{i,j}^{n+1}}{\sqrt{(\phi_{i+1,j}^n - \phi_{i-1,j}^n)^2/(2h)^2 + (\Delta_+^y\phi_{i,j}^n)^2/(h^2)}}\right)$$

$$\left. -\nu - \lambda_1\left(u_{0,i,j} - c_1(\phi^n)\right)^2 + \lambda_2\left(u_{0,i,j} - c_2(\phi^n)\right)^2\right] \quad (12)$$

After solving the above equations, the results of two-region ϕ segmentation are as follows:

$$\begin{cases} R_1 = uH(\phi), \\ R_2 = u(1 - H(\phi)) \end{cases} \quad (13)$$

At the right end of the above equation is each limiting factor in the evolution. The first term is the length of the curve and the second is the area around the curve. When the above equation is solved by the difference method, the length and area of the curve decrease and finally a smooth curve is obtained. As the segmentation algorithm gets closer to the target edge, the image grays are similar and the difference between the inner and outer grays is almost zero. It will deviate from the symbolic distance function and needs to be re-initialized, greatly increasing the number of iterations. As a result, the image segmentation time of this model increases and easily leads to incomplete segmentation.

Therefore, the energy term (Jiang *et al.*, 2008):

$$F_1(c_1, c_2, j) = \mu \int_\Omega |\tilde{N}H(j)|\, dxdy + \nu \int_\Omega |H(j)|\, dxdy + \lambda_1 \int |H(j)||u_0(x,y) - c_1|^2\, dxdy + \lambda_2 \int (1 - |H(j)|)|u_0(x,y) - c_2|^2 dxdy \quad (14)$$

The level set function is added to the sign distance function:

$$F_2(\phi) = \frac{1}{2}\beta \int_\Omega (|\nabla\emptyset| - 1)^2 dxdy \quad (15)$$

Considering the low utilization rate of the CV model on the edge information of the image, the step difference of the image before and after segmentation is added. The level set is as follows:

$$F_3(b_1, b_2, \phi) = \alpha_1 \int_{inside(c)}(|\nabla u_0(x,y)| - b_1)^2\, dxdy + \alpha_2 \int_{outside(c)}(|\nabla u_0(x,y)| - b_2)^2\, dxdy \quad (16)$$

The improved CV model can be obtained as follows:

$$F = F_1 + F_2 + F_3 \tag{17}$$

The evolution equation can be obtained from the gradient downflow equation as follows:

$$\frac{\partial \varphi}{\partial t} = -\frac{\partial F}{\partial \varphi} = \mu \delta(\varphi) div\left(\frac{\nabla \varphi}{|\nabla \varphi|}\right) + \beta div\left((1 - \frac{1}{|\nabla \varphi|})\nabla \varphi\right)$$
$$+ \delta(\varphi)(\alpha_2 (|\nabla u_0(x,y)| - \alpha_1 (|\nabla u_0(x,y)|$$
$$+ \lambda_2 (u_0 - \lambda_1 (u_0 - v) \tag{18}$$

The AOS algorithm is an effective method for solving curve evolution problems based on geometric active contour models and means curvature (Xie and Mirmehdi, 2008). The basic idea is to decompose a complex multidimensional problem into several simple one-dimensional problems. After solving each one-dimensional problem separately, an approximate solution to the multidimensional problem can be obtained by taking the average. In the CV model, the AOS operator is used for the numerical calculation to improve the efficiency of the curve evolution solution. The improved CV model includes the simplification of Heaviside and Dirac functions, as well as the construction of a numerical calculation method for the curvature of the image. This makes it more robust to the initial contour position and is able to handle images with noisy, blurred, and discontinuous edges. Using the AOS operator, the improved CV model can segment images more effectively and improve the accuracy and efficiency of segmentation. Adding the AOS operator to the numerical computation yields the evolution formula:

$$\Phi^{n+1} = \frac{1}{2}\sum_{l \in (x,y)} \left(I - 2\tau A_l(\Phi^n)\right)^{-1}(F'(\Phi) + \Phi^n) \tag{19}$$

The MLP-CV model algorithm is shown in Table (1).

Table 1: Algorithm of MLP-CV model

Algorithm: MLP-CV model algorithm
Input: Linearly separable training dataset D(x), segmented image I, number of training rounds, MLP network N_{epoch} $f(x)$
Output: segmentation Region C
Initialize MLP
for $t = 1: N_{epoch}$ do
$\qquad$ Calculate L_1 using $H(y, f(x))$
$\qquad$ Calculate L_2 using $L_\delta(y, f(x))$
$\quad$ Update $f(x)$
End for
$I_{seg} = f(I)$
for $t = 1: N_{iter}$ do
for (x,y) in the octal neighborhood do
Calculate f_x using $\left(I_{seg} - 2\tau A_x(\Phi^n)\right)^{-1}(F'(\Phi) + \Phi^n)$
$\quad$ Calculate f_y using $\left(I_{seg} - 2\tau A_y(\Phi^n)\right)^{-1}(F'(\Phi) + \Phi^n)$
$\qquad$ Update Φ using $\Phi^{n+1} = \frac{1}{2}\left(\Phi_x^{n+1} + \Phi_y^{n+1}\right)$
End for
End for
Output: C = Φ

Experiment

A series of experiments will be conducted to evaluate the effectiveness of the proposed method. First, the problem to be validated is presented; then, the experimental setup is described; finally, the experimental results and analysis are given.

Problems to be Verified

The effectiveness of the proposed method is verified by answering the following two questions:

(1) How effective is the MLP-CV method?
(2) Can the method improve the detection efficiency of lung nodules?

Data Sets

LUNA16 dataset is a subset of the LDC-IDRI dataset, excluding lung nodules with slice thicknesses greater than 3 mm and less than 3 mm. It includes data from 888 low-dose lung CT images, with a total of 1,186 lung nodules.

Experimental Environment

Intel(R) Core(TM)i5-11400H @ 2.70GHz 2.69GHz; RAM: 32GB; Graphics: NVIDIA GeForce RTX 3050 Laptop GPU; Operating system: Windows 11; Software: MATLAB R2021a.

Experiment Setup

First, mhd is read and Matric Transform is used to determine whether the 3D CT value matrix needs to be flipped in the x and y directions and then the 3D CT matrix is returned. After that, the CT image data is preprocessed and normalized. CT value is a unit of measurement to determine the density of human organs, with a unit HU. Finally, the CT image is visualized and the location of the nodule is marked. Since the CT image is a single-channel image, it should be converted to RGB format before saving; otherwise, it will be an all-black image. 12,000 CT images from LUNA16 are selected as the dataset, with 80% being the training set, 10% being the testing set and 10% being the validation set.

Results

About Question 1

Five *Precision* indexes including Accuracy, precision, specificity, and Area under the Curve (AUC) under the Receiver Operating Characteristic (ROC) curve are selected to measure the efficiency of segmentation. The accuracy rate is defined as follows:

$$Accuracy = \frac{TP + TN}{TP + FP + TN + FN} \tag{20}$$

Table 2: Iterations at 10 intervals

Number of iterations	10	20	30	40	50	60	70	80	90	100
Accuracy of training and	0.9910	0.9361	0.9357	0.9351	0.9812	0.9767	0.9738	0.9907	0.9934	1
testing	0.9907	0.9339	0.9338	0.9330	0.9802	0.9763	0.9738	0.9906	0.9930	1
AUC value	0.98081	0.92434	0.92418	0.92343	0.97036	0.96655	0.96398	0.98073	0.98313	0.9901

Precision is defined as:

$$Precision = \frac{TP}{TP+FP} \qquad (21)$$

Specificity is defined as:

$$Specificity = \frac{TN}{TN+FP} \qquad (22)$$

Where *TP* is a positive sample; *FP* is a false positive; *TN* is a negative sample and *FN* is a false negative. In addition, the closer the AUC value is to 1.0, the higher the veracity of the segmentation method.

In the experiment, when the iteration is 10 times (1 time represents 1000 times), the training accuracy is 99.10%; the testing accuracy is 99.07% and the AUC of the ROC curve is 0.98081. As the number of experiments increases, the accuracy of training and testing will change. After 100 epoch iterations, the accuracy of training and testing can reach 100% and the AUC of the ROC curve is 0.9901. The iterations are shown in Table (2).

As shown in Table (2), it can be found that the accuracy shows a higher score at the 10th epoch iteration. As the number of iterations increases, the accuracy decreases first and then increases. The number of iterations will affect the results. Fig. (4) shows the results of 100 iterations. Table (3) shows the AUC values of the training, testing, and ROC curves. The 3rd, 5th, 7th, 15th, 21st, 33rd, 41st, 47th, 48th, 59th, 61st, 65th, 68th, 85th, 97th and 99th epochs all have the same results as the 100th iteration. The accuracy of 17 times is100%, with an average accuracy of 0. The accuracy of testing is 0.9642 and the average AUC is 0.9547. Therefore, the segmentation algorithm of the MLP-CV model is feasible. The accuracy in the 3rd epoch is 100%, which accelerates the segmentation. This segmentation method is fast and effective.

Figure (5) shows the effect diagram of lung nodule segmentation using the MLP-CV model. Green indicates the segmented nodules.

Figure (6) shows the loss function. As the number of experimental iterations increases, the image becomes more stable.

Figure (7) shows the AUC value of the ROC curve in the 3rd, 30th, 60th, and 100th iterations. Figure (7) shows the confusion matrix and Fig. (8) shows the detection results. The 3rd and 100th iterations have the same results, with an AUC value of 0.9901. The area under the ROC curve is close to 1, indicating a high-quality detection method.
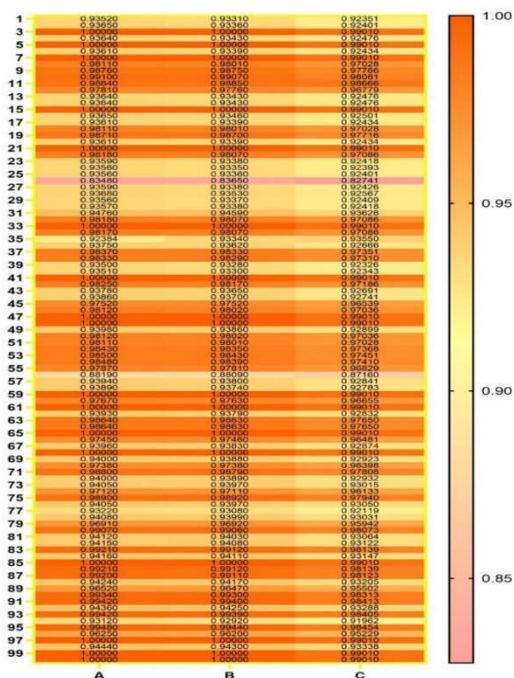
Fig. 4: Different iterations with 1 interval
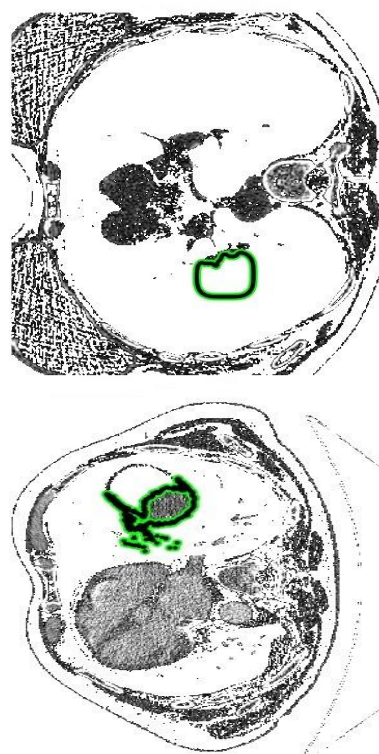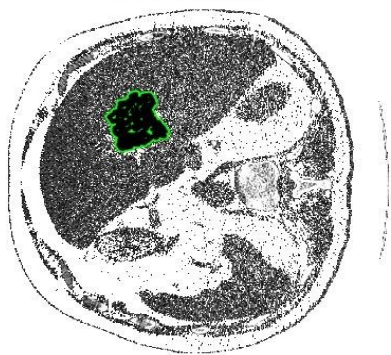
Fig. 5: Diagram of Segmentation effect
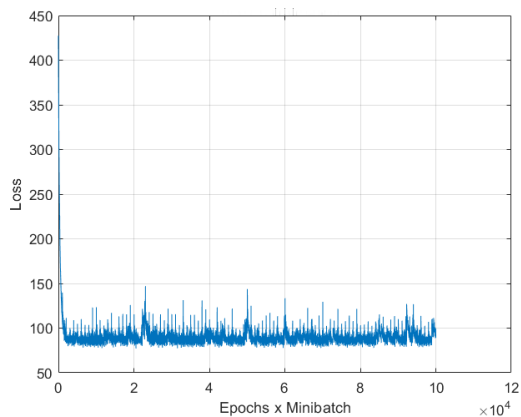
Fig. 6: Diagram of the loss function
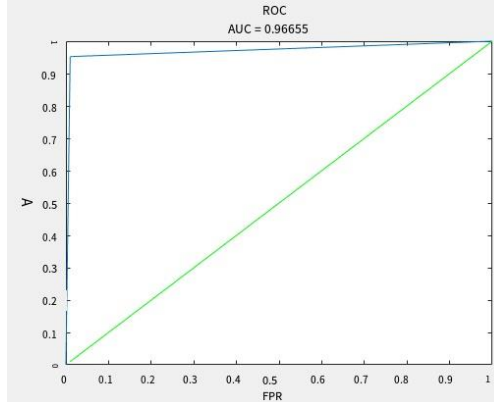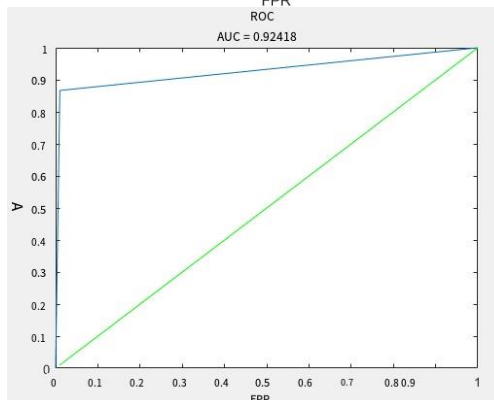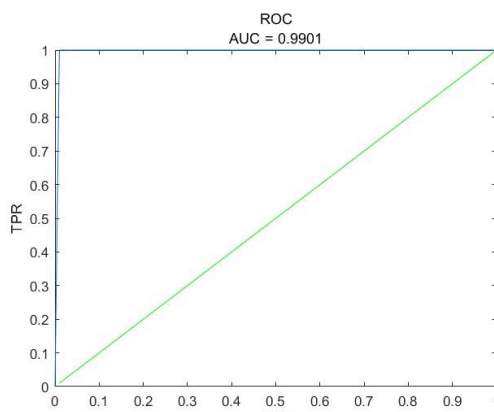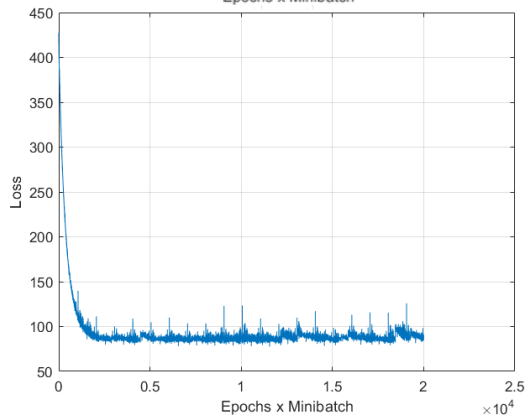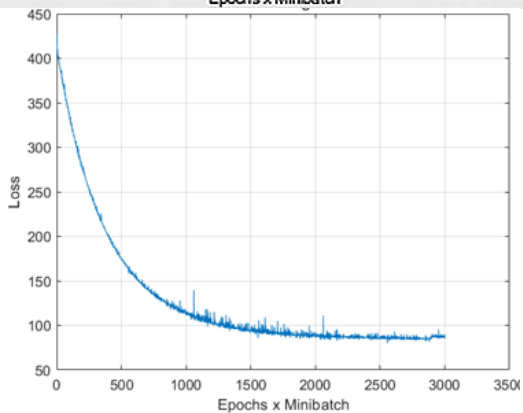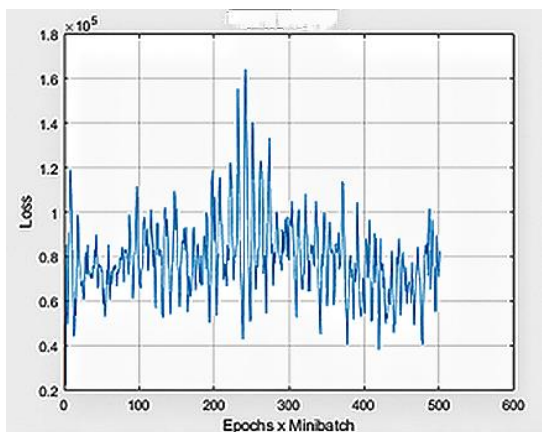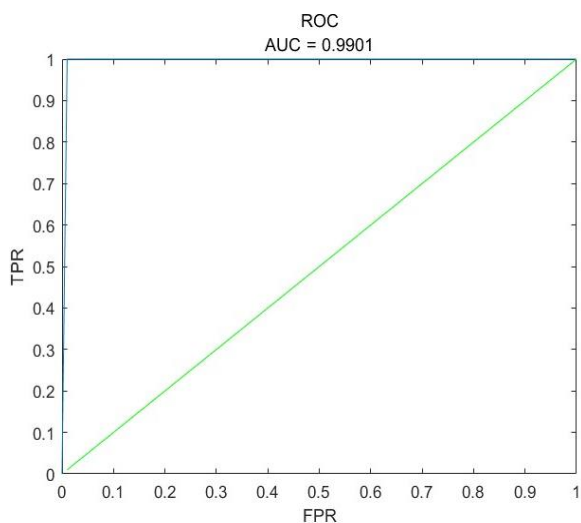
Fig. 7: AUC value of ROC curve
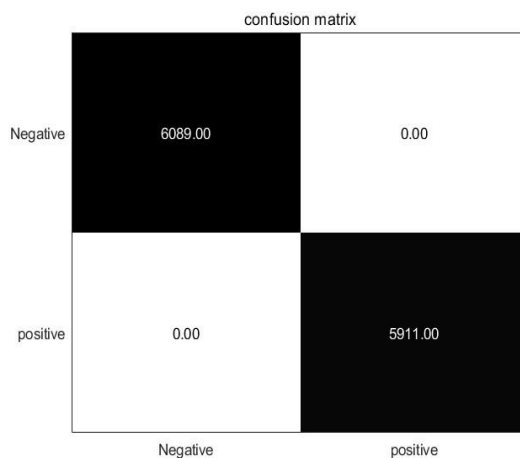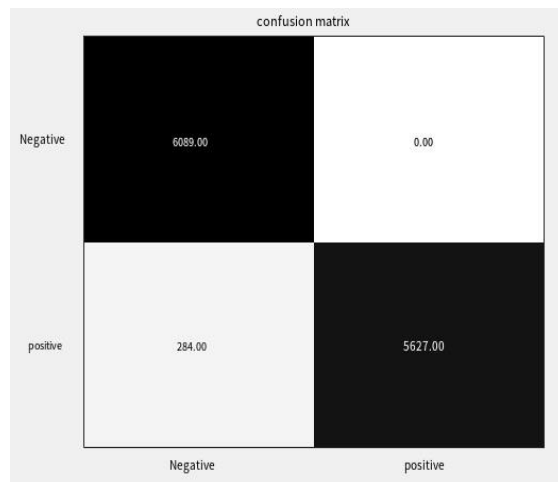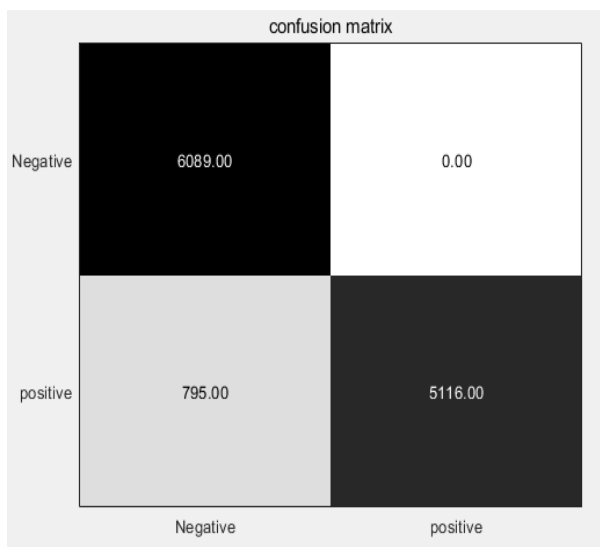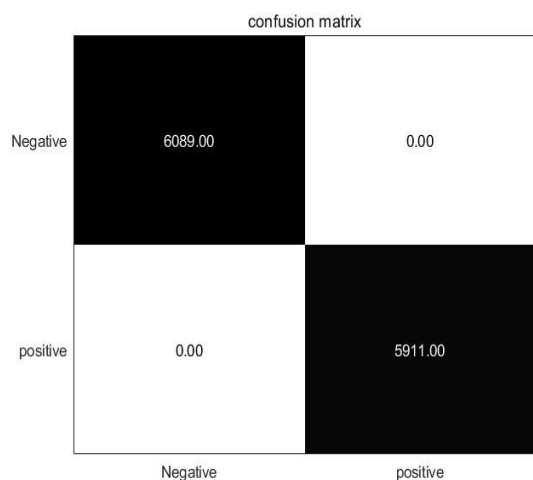
Fig. 8: Confusion matrix

The confusion matrix for 3, 30, 60, and 100 iterations is shown in Fig. (8), where 3 and 100 iterations are combined. The results are consistent, that is, the accuracy and specificity of the 1st and 4th graphs are both 1; the accuracy of the other two graphs are 0.8655 and 0.9520 and the specificity is 0.8845 and 0.9407, respectively.

The detection results for the 3rd, 30th, 60th, and 100th iterations are shown in Fig. (9), where the nodes of the 3rd round and the 100th iteration have the same results. That is the actual classes in Figs. (1 and 4) are exactly the same as the detected classes. There are different degrees of deviation in Fig. (2 and 3) and Figs. (3) is better than Fig. (2) after comparison.

About Question 2

As shown in Table (3), the LUNA16 dataset is compared with other methods to show how well lung nodule detection is. The MLP-CV model is good at detecting lung nodules and accuracy improvement.
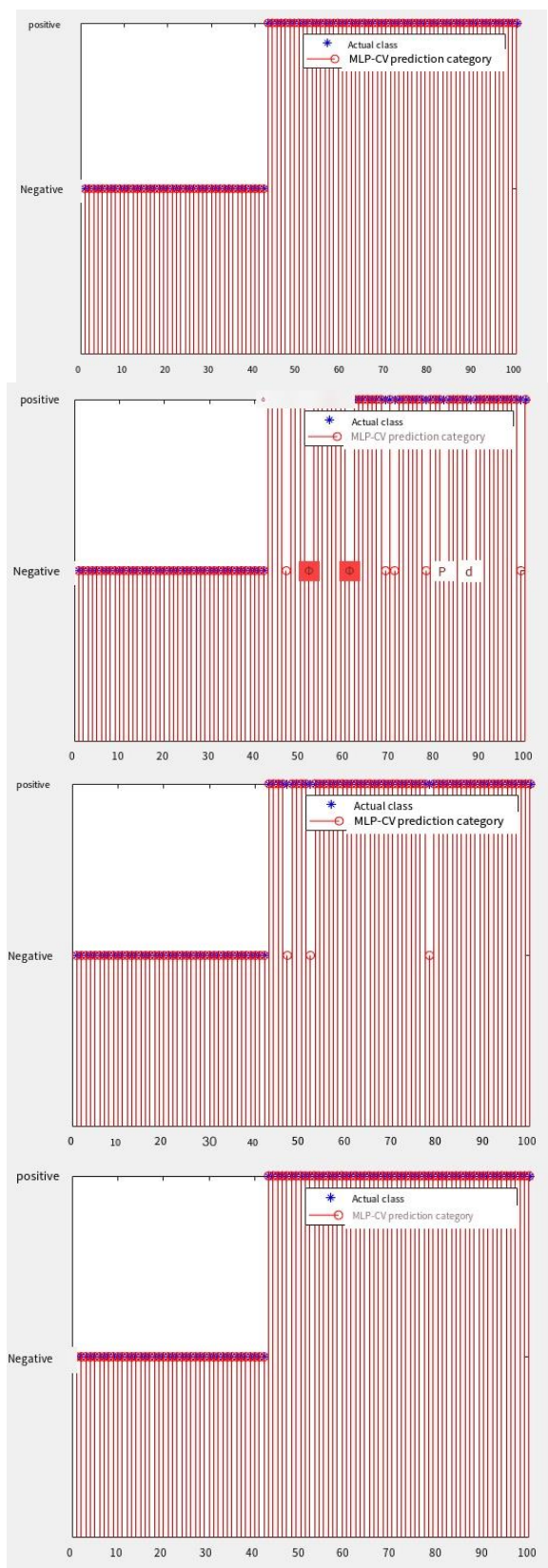
Fig. 9: Detection results

Table 3: Comparison of different models

Methods	Accuracy rates
MLP-CV model	0.9642
Model 1 (Yue *et al.*, 2022)	0.9474
Model 2 (Cao *et al.*, 2022)	0.8880
Model 3 (Liang *et al.*, 2022)	0.9000
Model 4 (Liu *et al.*, 2022)	0.9470

Discussion

The experimental results show that the algorithm has high accuracy and efficiency. However, there are some shortcomings in the algorithm and potential limitations of the algorithm are explored as follows: The experiments are performed only on the LUNA16 dataset, which cannot cover all types of lung nodules and lesions. The algorithm may perform differently on more diverse datasets. As the experiment mentions that 100% accuracy is achieved by the third iteration, this may indicate that the model is overfitted on the training set. Although high accuracy is also achieved on the test set, more datasets are needed to validate the generalization of the model. The combination of the MLP and CV models may increase the complexity of the model, which may result in higher computation and longer training times. This may be a focus in resource-constrained environments. The performance of MLP and CV models largely depends on parameter settings and model performance is overly sensitive to initial parameter selection. Experimental results need to be clinically validated to further confirm their validity. Comparisons with actual clinical data will provide more information on the usefulness of the models.

Conclusion

Aiming at the problem of low accuracy of lung nodule segmentation and subsequent classification in pneumoconiosis detection, an MLP-CV algorithm is proposed. It first trains the MLP to recognize the lung nodules and obtain their area and then outputs the initial contour containing the nodules. After that, these nodules are automatically segmented by using the improved CV model to obtain fast and accurate detection of lung nodules.

The LUNA16 dataset is segmented to detect lung nodules by fusion and improvement of MLP and CV models. 100 epochs of training and testing are performed, with 17 epochs achieving 100% accuracy, with an average accuracy of 0.9642. The program can reach 100% accuracy only after the third epoch, indicating the fastness and effectiveness of the detection method.

There is still room for improvement in the current work due to a small dataset and a risk of overfitting. In the future, we will attempt testing on more datasets to improve the accuracy of lung nodule detection, explore how to quickly classify lung nodules, and further test and examine them clinically to provide the diagnostic basis for doctors.

Acknowledgment

Many thanks to the reviewers for their constructive comments, which have helped to improve this paper.

Funding Information

Ethics

Authors should address any ethical issues that may arise after the publication of this manuscript.

Conflict of Interest

No potential conflict of interest was reported by the authors. The author declares that there is no conflict of interest, financial or non-financial, related to the content of this article.

References

Abbas, K. K., & Li, X. (2024). Locally Enhanced Chan-Vese Model with Anisotropic Mesh Adaptation for Intensity Inhomogeneous Image Segmentation. *Intelligent Systems and Applications*, 111–127. https://doi.org/10.1007/978-3-031-47715-7_9

Akbari, Y., Hassen, H., Al-Maadeed, S., & Zughaier, S. M. (2021). COVID-19 Lesion Segmentation Using Lung CT Scan Images: Comparative Study Based on Active Contour Models. *Applied Sciences*, *11*(17), 8039. https://doi.org/10.3390/app11178039

Annarumma, M., Withey, S. J., Bakewell, R. J., Pesce, E., Goh, V., & Montana, G. (2019). Automated Triaging of Adult Chest Radiographs with Deep Artificial Neural Networks. *Radiology*, *291*(1), 196–202. https://doi.org/10.1148/radiol.2018180921

Bengio, Y., Courville, A., & Vincent, P. (2013). Representation Learning: A Review and New Perspectives. *IEEE Transactions on Pattern Analysis and Machine Intelligence*, *35*(8), 1798–1828. https://doi.org/10.1109/tpami.2013.50

Cao, Z. G., Li, R., & Zhang, Z. T. (2022). Lung medical image recognition based on deep learning (In Chinese. *Journal of Qiqihar University (Natural Science Edition*, *38*(2), 44–49. https://doi.org/10.3969/j.issn.1007-984X.2022.02.009

Chan, T. F., & Vese, L. A. (2001). Active contours without edges. *IEEE Transactions on Image Processing*, *10*(2), 266–277. https://doi.org/10.1109/83.902291

Cootes, T. F., Taylor, C. J., Cooper, D. H., & Graham, J. (1995). Active Shape Models-Their Training and Application. *Computer Vision and Image Understanding*, *61*(1), 38–59. https://doi.org/10.1006/cviu.1995.1004

Desai, M., & Shah, M. (2021). An anatomization on breast cancer detection and diagnosis employing multi-layer perceptron neural network (MLP) and Convolutional neural network (CNN). *Clinical EHealth*, *4*, 1–11. https://doi.org/10.1016/j.ceh.2020.11.002

Dong, B., Weng, G., & Jin, R. (2021). Active contour model driven by Self Organizing Maps for image segmentation. *Expert Systems with Applications*, *177*, 114948. https://doi.org/10.1016/j.eswa.2021.114948

Gao, H., Li, J., Shen, N., Liu, L., Yang, Y., Hu, P., & Lu, W. (2024). An improvement method for pancreas CT segmentation using superpixel-based active contour. *Physics in Medicine & Biology*, *69*(10), 105027. https://doi.org/10.1088/1361-6560/ad3e5c

Jiang, N., Zhang, R. K., Pu, L. X., & Chen, W. J. (2008). Research of Fast Approach for Chan-Vese Model (In Chinese). *Journal of University of Electronic Science and Technology of China*, *37*(5), 705–708. https://doi.org/10.3969/j.issn.1001-0548.2008.05.017

Kass, M., Witkin, A., & Terzopoulos, D. (1988). Snakes: Active contour models. *International Journal of Computer Vision, 1*(4), 321-331. https://doi.org/10.1007/BF00133570

Li, G. (2022). Research on interactive image segmentation. *Hubei: Central China Normal University, China*. https://doi.org/10.27159/d.cnki.ghzsu.2022.000088

Liang, F. E., Zhang, W., Lv, S. S., Gu, X., & Liu, D. H. (2022). Research on Lung Nodule Segmentation Based on V-Net Model (In Chinese). *Modern Information Technology*, *6*(19), 71–74. https://doi.org/10.19850/j.cnki.2096-4706.2022.19.018

Liu, Y. B., Liu, G. Z., Shi, C., & Xu, C. H. (2022). Pulmonary Nodules Detection Algorithm Combining Multi-view and Attention Mechanism (In Chinese). *Journal of Harbin University of Science and Technology*, *27*(6), 115–123. https://doi.org/10.15938/j.jhust.2022.06.014

Lyu, S., Cheng, J., Wu, X., Cui, L., Chen, H., & Miao, C. (2022). Auxiliary Learning for Relation Extraction. *IEEE Transactions on Emerging Topics in Computational Intelligence*, *6*(1), 182–191. https://doi.org/10.1109/tetci.2020.3040444

Ma, D., Liao, Q., Chen, Z., Liao, R., & Ma, H. (2019). Adaptive local-fitting-based active contour model for medical image segmentation. *Signal Processing: Image Communication*, *76*, 201–213. https://doi.org/10.1016/j.image.2019.05.006

Ma, P., Yuan, H., Chen, Y., Chen, H., Weng, G., & Liu, Y. (2024). A Laplace operator-based active contour model with improved image edge detection performance. *Digital Signal Processing*, *151*, 104550. https://doi.org/10.1016/j.dsp.2024.104550

Manaswi, N. K. (2018). Multilayer Perceptron. *Eep Learning with Applications Using Python : Chatbots and Face, Object and Speech Recognition with TensorFlow and Keras*, 45–56. https://doi.org/10.1007/978-1-4842-3516-4_3

Mumford, D., & Shah, J. (1989). Optimal approximations by piecewise smooth functions and associated variational problems. *Communications on Pure and Applied Mathematics*, *42*(5), 577–685. https://doi.org/10.1002/cpa.3160420503

National Health Commission of the People's Republic of China. (2022). Statistical Bulletin on Health Development in China 2021 (In Chinese). *Chinese Journal of Practical Rural Doctors*, *29*(9), 1–11. https://doi.org/10.3969/j.issn.1672-7185.2022.09.001

Peng, J. X. (2019). Research on damage identification of segmental prefabricated concrete beams based on acoustic emission technology (In Chinese). *Beijing Jiaotong University, China*. https://doi.org/10.26944/d.cnki.gbfju.2019.000194

Rosenblatt, F. (1958). The perceptron: A probabilistic model for information storage and organization in the brain. *Psychological Review*, *65*(6), 386–408. https://doi.org/10.1037/h0042519

Shi, Q., Yin, S., Wang, K., Teng, L., & Li, H. (2022). Multichannel convolutional neural network-based fuzzy active contour model for medical image segmentation. *Evolving Systems*, *13*(4), 535–549. https://doi.org/10.1007/s12530-021-09392-3

Xiang, Y., Sun, Y., Liu, Y., Han, B., Chen, Q., Ye, X., Zhu, L., Gao, W., & Fang, W. (2019). Development and validation of a predictive model for the diagnosis of solid solitary pulmonary nodules using data mining methods. *Journal of Thoracic Disease*, *11*(3), 950–958. https://doi.org/10.21037/jtd.2019.01.90

Xie, X., & Mirmehdi, M. (2008). MAC: Magnetostatic Active Contour Model. *IEEE Transactions on Pattern Analysis and Machine Intelligence*, *30*(4), 632–646. https://doi.org/10.1109/tpami.2007.70737

Yan, J., Wang, X., Cai, J., Qin, Q., Yang, H., Wang, Q., Cheng, Y., Gan, T., Jiang, H., Deng, J., & Chen, B. (2022). Medical image segmentation model based on triple gate MultiLayer perceptron. *Scientific Reports*, *12*(1), 6103. https://doi.org/10.1038/s41598-022-09452-x

Yue, Q., Yan, J. Y., & Wang, S. (2022). Automatic Detection of Pulmonary Nodules in Low-dose CT Images Based on Improved CNN (In Chinese). *Computer Science*, *49*(S1), 54–59. https://doi.org/10.11896/jsjkx.210400211

Zhang, P. (2002). *Research on integrated acoustic emission signal processing platform*.